npj Quantum Information

https://doi.org/10.1038/s41534-026-01209-y

Article in Press

Integration of a single photon source with a fibre-compatible photonic waveguide

Received: 26 September 2025

Accepted: 22 February 2026

Cite this article as: Broussier, A., Muhammad, M.H., Rahbany, N. *et al.* Integration of a single photon source with a fibre-compatible photonic waveguide. *npj Quantum Inf* (2026). https://doi.org/10.1038/s41534-026-01209-y

Aurélie Broussier, Muhammad H. Muhammad, Nancy Rahbany, Abdelhamid Hmima, Paul Robineau, Cyrille Vezy, Régis Déturche, Antoine Kevorkian, Sylvain Blaize & Christophe Couteau

Integration of a single photon source with a fibre-compatible photonic waveguide

Aurélie Broussier[1x], Muhammad H. Muhammad[1,2+], Nancy Rahbany[3], Abdelhamid Hmima[1], Paul Robineau[1=], Cyrille Vezy[1], Régis Déturche[1], Antoine Kevorkian[2], Sylvain Blaize[1], Christophe Couteau[1,4*]

[1]Laboratory Light, nanomaterials and nanotechnologies-L2n, Université de Technologie de Troyes-UTT & CNRS UMR 7076, 12 rue Marie Curie, 10004 Troyes Cedex, France

[2]Teem Photonics, 61 Chemin du Vieux Chêne, 38246 Meylan, France

[3]Department of Physics and Astronomy, Faculty of Natural and Applied Sciences, Notre Dame University-Louaize, Zouk Mosbeh, Lebanon

[4]EUT+ Institute of Nanomaterials and Nanotechnologies EUTINN, European University of Technology, European Union, Troyes, France

[*]Corresponding author: christophe.couteau@utt.fr
[x]Currently at FEMTO-ST Institute, Besançon, France
[+]Currently at Synopsys photonics solutions, France
[=]Currently at LASIRE, UMR 8516 CNRS-Université de Lille, Lille. France

Abstract

The integration of a single photon source based on a solid-state emitter with a photonic structure remains challenging and specifically when it comes to be compatible with optical fibres. It is important to do so for quantum technologies where single photon sources constitute building blocks for many technologies. In this work, we demonstrate the integration of a single photon source, made of a colloidal semiconductor nanocrystal, with a photonic structure made of a glass waveguide obtained by the ion-exchange technique, which is a fibre-compatible platform used in telecom photonics. Using surface functionalisation and a secondary waveguide of titanium dioxide, we manage to couple single photons from the nanoemitter to the optical waveguide. We observe the single photon character is preserved and demonstrates a 1.2 Purcell factor. A coupling efficiency over 25 % is expected thanks to the titanium dioxide secondary waveguiding layer, compared to around 2 % obtained for simply positioning the nanocrystal on top of the waveguide alone. The optical waveguide is then pigtailed to an optical fibre to demonstrate a first proof of principle of an integrated single photon source at room temperature with a fibre-compatible platform made of glass with a coupling efficiency increase of 2.8.

Introduction

Optical emitters being able to provide single photons are relevant for quantum technologies in general[1,2], for quantum communications in particular. Recently, it has been shown that single photon emission surpasses weak coherent-states in quantum key distribution further demonstrating the importance of single photon sources for quantum communications[3]. We refer the reader to Labonté *et al.*, for instance, for further reading on QKD and integrated optics ref. 4 and for instance to ref. 5 for a review on integrated photonics for quantum technologies. It is thus of paramount importance to be able to efficiently couple such quantum emitters (emitting single[6,7], indistinguishable[8] or entangled photons[9]) with photonic structures such as waveguides[10,11], interferometers[12] and optical cavities[13] in order to be able to scale-up for any practical purposes. Several platforms and approaches for quantum communications are currently explored where quantum emitters and photonics structures are put together although most of them are effective at low temperatures (see for instance ref. 14 for colour centres in Si or ref. 15 for epitaxial quantum dots). Only few platforms work at room-temperature and previous works have been done with

single colour centres in photonic crystal diamond[16] or with single DBT molecules coupled to gold plasmonic waveguides are also being studied[17]. Waveguides made of silicon nitride are being investigated using intrinsic single photon emitters[18] or with colloidal quantum dots coupled to ring resonators[19]. In terms of emission of single photons at room temperature, single photons were also obtained from defects in 2D materials coupled to silver plasmonic nanowires in previous works[20].

So far though, it has been evidenced difficult to bring together quantum emitters which are usually nanosized objects and 'macro' photonic-ready platforms that could be compatible with optical fibres. The closest work we are aware of, is the work by Alvarez *et al.* where colloidal quantum dots have been coupled to laser-written glass waveguides but this was not at the single photon level[21].

In this work, we aim to explore a new path towards bridging the "nano" to the "macro" world by connecting optically a nanosource of light with a conventional optical waveguide (WG). Our method paves the way towards scaling-up to several quantum emitters by tackling light-matter interfacing between photons and nanosources of light on a single optical platform. Being able to scale-up is at the heart of quantum networks[22] and small-scale quantum photonics simulators[23]. This differs from the usual approach of getting the greatest light extraction from nanostructures on a substrate[24]. Here we use the substrate as an active element of the device which can be seen as an optical bus.

Fig. 1 is a schematic of our system where we have the photonics structure made of a semi-buried optical waveguide (using the so-called ion-exchange method[25,26]) made of glass and the quantum emitter (in our case a colloidal quantum dot or nanocrystal-NC) on top as the single photon emitter. In between, a secondary waveguide has been fabricated, made of a high-refractive index material, in our case titanium dioxide (TiO_2), in order to have a smooth adiabatic coupling of the nanosource to the micro-size waveguide underneath.

Results

The single photon emitter

In order to realise our integrated single photon source working at room temperature as a first proof of principle, it is necessary to use an emitter that emits single photons reliably and which does not require low temperatures. Only few emitters are relevant as single photon emitters, such as nanodiamonds[27,28], single molecules[29] or nanocrystals[30]. We use NCs as we find that more than 90 % of them are single photon emitters. The nanocrystals are core/multishell CdSe/CdS/CdZnS/ZnS NCs synthesised[31] in-house (See Methods Section) and are used in this work. Fig. 2a presents the typical absorption (dash orange) and emission (orange) of the NCs. We clearly see the excitonic absorption peak at 575 nm and the emission is at 610 nm (with a Full Width at Half Maximum FWHM = 25 nm). The excitation of the emission was obtained with a pulsed laser at 532 nm with a pulse rate of 5 MHz. The absorption and the fluorescence were respectively normalized to 1 for the exciton absorption peak and to the maximum of the emission. Fig. 2b presents a typical photon antibunching result of a single NC on a standard glass substrate showing a $g^{(2)}(0) = 0.14 \pm 0.05$ below 0.5 and thus ensuring we have single photon emitters. Most of the background value of the $g^{(2)}(0)$ is due to the use of a broadband filter centered at 618 nm with a rather wide FWHM of 50 nm. This brings some residual noise represented in gray in Fig. 2a. If we take into consideration this noise as well as the avalanche photodiodes (APDs) dark counts, the value would go down to $g^{(2)}(0) = 0.04 \pm 0.015$. We obtained the grey area by averaging the light detected from the laser placed on the sample where there is no NCs.

The photonic platform

For the realisation of our integrated single photon source, we use glass waveguides fabricated with the so-called ion-exchange technique[25] (IEWs). In Fig. 1, one can see that the coupling of the nanosources of light to the WGs is done at the surface as the waveguides are half-buried and thus allowing to interact with whatever emitter placed at their surface. IEWs are made by the exchange of sodium ions in glass with silver ions coming from a silver salt placed at the surface under heating. The exchange of ions has the consequence of changing the refractive index of the glass locally going from 1.5 or so, to 1.57 or so and thus resulting in a refractive index difference on the order of $\Delta n = 0.07$ which is enough to provide a good optical confinement of guided modes within the region of higher index due to the presence of silver ions. Using this technique, it is also possible to fabricate fully or partially buried WGs. This is one of the main advantages of using IEWs (see Ref. 26 for more on such optical WGs) as opposed to laser-written waveguides[32] for instance which can only be within inside the bulk glass and thus cannot interact with a nanosource on top. Nevertheless, placing a single NC at the surface of an IEW is not enough to get a significant coupling of the photons emitted by the NC into the guided modes of the glass waveguides (Fig. 1). Our numerical simulations show that around 1.6 % of the light emitted by an NC placed on top of the waveguide would be coupled into the IEW for a dipole (with an averaged orientation) placed at the top. It is thus important to improve the coupling of the quantum emitters to the WGs at the surface of the IEWs[33]. For this, the use of a high refractive index layer in between the NC and the IEW allows a much better coupling[10,11]. As shown in Fig. 1, we use a layer of titanium-dioxide (TiO_2) with an optical index of 2.2 (at the wavelength of 610 nm, corresponding to the emission of our NCs). Moreover, TiO_2 is a transparent material for most of the visible region where the NCs emit. In order to optimise the dimensions of the TiO_2 waveguide placed at the surface, 3D-finite difference time domain (FDTD) numerical simulations were carried out with the ion-exchange waveguide (taken with a refractive index of 1.57) in a glass substrate (taken with a refractive index of 1.5) as the one depicted in Fig. 1. This structure IEW + TiO_2 has been optimised to have the best coupling efficiency. At the end, the estimated coupling efficiency from the simulation for the on-chip single photon source would be 25.9 %. Numerical simulations were also done to study the light propagation through our photonic structure, and the optimised parameters for the TiO_2 'strip' waveguide at the surface for a wavelength of 610 nm were found to be as follows: width $w = 190\ nm$, height $h = 175\ nm$ and length $L = 35\ \mu m$. We must already point out that due to surface roughness of the TiO_2 waveguides after fabrication, we did get at the most an increase of 2.8 of the light coupling thanks to the TiO_2 layer (and not a factor of 12 to 13 or so, expected from the simulations). This can be observed from Supplementary Figure 3 on an ensemble measurement of many NCs.

Fabrication of the photonic structure

The fabrication of the hybrid structure with the IEW and the TiO_2 strip waveguide at the surface was done in several steps. We first start from the glass waveguide which is cleaned thoroughly. In order to produce the TiO_2 strip waveguide, we use the electron-beam (e-beam) lithography technique. We start by depositing a layer of the well-known resin poly (methyl methacrylate) (PMMA) by spin coating it on the IEW sample. As the waveguides can be seen with an electron microscope, we center the electron beam in the middle of the guide. Our lithography system allowed us to write several guides at the same time with a spacing of 50 µm between them. The PMMA layer was then carved out via electron-beam lithography followed by 1 min development in methyl isobutyl ketone (MIBK) and 1 min in isopropanol). We then deposit the 175 nm ($h = 175\ nm$ being the optimised calculated layer) layer of TiO_2 by evaporation. Typically, after the metal evaporates, the PMMA resin is lift-off to achieve the rectangular structure. We decided not to perform this at this stage, but rather immediately after surface

functionalisation of the TiO_2 layer with NCs. By proceeding in this way, we ensure that the NCs via the silanes are attached only at the TiO_2 guides. The next step is thus to place the nanocrystals (preferably single ones) on top of the TiO_2 waveguides and only there. Fig. 3 presents the fabrication steps using the surface functionalisation method[34]. These were necessary steps in order to realise the placement of NCs on TiO_2 layers only. For this, the sample made of the TiO_2 strip waveguide on the IEW was placed in a silane solution (3-Mercaptopropyl)-triethoxysilane (MPTES), in anhydrous ethanol + 5% H_2O, concentration between 2 to 5%) to make the "connection" between the sample surface and the quantum emitters, *i. e.* the NCs. The sample was left for 12 hours in this solution before being removed from the silane solution and rinsed with ethanol. Once the sample surface has been functionalised with silane, the sample is then placed in a toluene solution containing the NCs for 30 s which was optimized to obtain on average a single monolayer of nanocrystals with a low concentration of 10 nM so that single NCs only would be attached to the surface[34]. During this step, the PMMA is removed completely and only the TiO_2 strips are left with the low concentration of NCs attached to them. At the end, 18 IEWs came out with TiO_2 strip waveguides on top after surface functionalisation of the NCs (See in Supplementary Section 1, Supplementary Figure 1 for an optical image and Supplementary Figure 2 for AFM images).

Optical characterisation

To characterise the IEW-TiO_2 structures with the nanocrystals on top, we use a home-made microphotoluminescence setup, depicted in Fig. 4. A pulsed or a continuous-wave (CW) laser emitting at 532 nm is focused on the sample through a 100x objective (NA = 0.95) on the surface. The emission from the emitters is then collected via the same objective. A 650 ± 75 nm bandpass filter is placed in front of the spectrometer to be able to cut the laser emission. For lifetime and $g^{(2)}$ autocorrelation measurements, a shorter 618 ± 25 nm bandpass filter was used. To find out if the emitter emits single photons, the light collected by the objective is sent to a 50/50 beam splitter placed before two single photon detectors (APDs) connected to a time-correlated single photon counting (TCSPC) system in order to realise the so-called Hanbury Brown and Twiss (HBT) experiment for checking whether an emitter emits single photons or not. A piezoelectric stage system (in x and y) makes it possible to realize a scan (maximum field of view of 60 µm by 60 µm) of the sample emission, thanks to the photon-counts coming from one of the detectors. This single photon detector is then connected to a home-made electronic converter which gives us a photoluminescence image of the top surface of the system such as the one in Fig. 5. This piezoelectric stage system then allows us to place the excitation at the desired position once the image of the surface is obtained and when a potentially relevant NC has been identified.

Fig. 5 shows a scan of an area of 10 µm by 40 µm with a step size of 0.5 µm of the surface of the sample where one TiO_2 waveguide is found (white small rectangle). The IEW can be seen between the two white lines with a width of about 2.5 µm to be seen. More intense points can be observed (green to yellow colours), in particular, the yellow point at the position of coordinates ~ 6 µm and ~ 16 µm. The other emitting points correspond to the fluorescence of the IEW in the range of 575 to 725 nm (which can thus be seen, through our bandpass filter) by the excitation at 532 nm due mostly to the silver ions contained in the ion-exchange WG[35].

On this waveguide, the 532 nm laser spot was then placed at the supposedly NC point level of the image from Fig. 5 thanks to the piezoelectric stage system. The black spectrum in Fig. 6a represents the emission from this point (the bright yellow point in Fig. 5) via the collection from the top microscope objective, excited by the 532 nm CW laser. On the black spectrum, an emission peak at 610 nm (FWHM ≈ 28 nm) is present. This peak corresponds to the emission of the NCs that we presented previously (Fig. 2a). On this spectrum, in addition to the NC emission we observe a weaker and broader peak centered around 680

nm. This broad peak corresponds to fluorescence coming from the IEW-TiO_2 structure. Indeed, when we place the laser directly on the TiO_2 structure on the guide, the blue spectrum of Fig. 6-a is obtained by the top detection from the objective. In fact, the waveguide fluorescence shows two broad peaks at 620 and 680 nm respectively (See Supplementary Section 2 and Supplementary Figure 3). These two peaks are attributed to the insertion of silver ions in the glass waveguide to form the IEW[36] (see Supplementary Section 2). The photoluminescence of the strip (white small rectangle) of TiO_2 directly on glass presented an emission peak at 675 nm[37] (see the pink curve in Supplementary Figure 3b). Thus, the peak at 620 nm is attributed to the silver ion luminescence alone while the peak at 680 nm has the contribution of silver ions and defects from the TiO_2 layer. This sample containing potentially a single NC on the photonic structure was then fibre-pigtailed (see inset of Fig. 6a). The red spectrum from Fig. 6a represents the emission spectrum coming out from the fibre of the photonic platform with a top excitation. We can observe that the background fluorescence from the silver ions in the IEW and from the TiO_2 layer is mostly filtered out and is not guided by the IEW. The NC emitter was then tested with our HBT interferometer to find out if it is truly a single photon emitter. The $g^{(2)}$ result under a pulsed laser excitation at 532 nm is shown in Fig. 6b. The obtained value of $g^{(2)}(0) = 0.24 \pm 0.1$ for the emission peak at zero delay is clear evidence that we have a single photon source from the NC emission. Once again, the non-ideal $g^{(2)}(0)$ result is due to the parasitic luminescence from the IEW and the TiO_2 strip as just discussed. After removal of the background light (grey area in Fig. 6b), we can obtain a value of $g^{(2)}(0) = 0.14$, which clearly proves the emission of a single photon. We studied other nanocrystals with more waveguides with a fibre output giving a $g^{(2)}(0)$ corresponding to a single photon emitter (see Supplementary Section 3).

To get an idea of the coupling between the single NC and the waveguide via the TiO_2 photonic structure, measurements of the lifetime of this NC were carried out. Fig. 7 represents the lifetime measurement under a 532 nm pulsed laser excitation at a 5 MHz repetition rate, respectively for NCs on a glass substrate alone (in black) and of a single NC on the photonic hybrid structure (in red) (see more in Supplementary Section 2). In the presence of the TiO_2 structure on the IEW, the lifetime of the NC decreases compared to its lifetime on the substrate reference. To validate the fluorescence decay rate, the data were fitted using a bi-exponential model according to the equation $I(t) = I_0 + A_1 e^{\frac{-t}{\tau_1}} + A_2 e^{\frac{-t}{\tau_2}}$. Using this fitted model, excited state lifetimes of $\tau_1 = 3.39\ ns$ and of $\tau_2 = 20.09\ ns$ for NCs on the glass substrate alone and excited state lifetimes of $\tau_1 = 3.05\ ns$ and of $\tau_2 = 16.53\ ns$ for a single NC on the photonic IEW/TiO_2 structure were found. The fact that two different lifetimes are observed with such values can be explained by some charged exciton states (for the short one of ~ 3 ns, due to Auger recombination) as well as neutral exciton states (for the longer one of ~ 20 ns) as observed previously[38]. The lifetime measurement represents the NC decay rate of the excited state. It thus includes the radiative Γ_{rad} and non-radiative Γ_{nr} decay rates $\Gamma = \Gamma_{rad} + \Gamma_{nr}$. From the lifetimes obtained on the different structures, the Purcell factor can be calculated as follows $P_f = \frac{\Gamma}{\Gamma_0} = \frac{\tau_0}{\tau}$, with τ_0 and τ representing respectively the averaged NC lifetime on a glass substrate and on the IEW/TiO_2 structure in our case. In the case of Fig. 7, a Purcell factor of 1.19 ± 0.01 was deduced for a single NC whereas simulations provided a Purcell Factor of 1.45. The discrepancy can come from a specific orientation of the dipole (whereas simulations are taken with an average orientation) or from a difference in the experimental optical coupling with structure, itself with some imperfections. This is however consistent with results obtained previously with a similar structure and an ensemble of NCs[10,11]. The Purcell factor of a single NC on the waveguide alone is 1.08 whereas simulations predict a value of 1.11. Thus, as expected, by adding a high

index structure of TiO_2 onto the waveguide, it is possible to increase the Purcell factor and to increase the coupling efficiency in the guide.

Discussion

In this paper, we have presented a fibered single photon source based on a hybrid photonic structure. The use of an ion-exchange glass waveguide makes it possible to have a fibered source emitting single photon at room temperature. The addition of the high index structure of TiO_2 to the emitter allows a better coupling into the waveguide of a factor of 12 to 13 or so obtained by numerical simuation and a factor of 2.8 was obtained experimentally due to surface roughness of the TiO_2 layer. The use of a plasmonic antenna will increase even more so this coupling with first simulation results showing coupling over 95 % in some cases[39]. In this work, we observe the contribution of luminescence from the silver ions of the waveguide as well as the luminescence from the TiO_2 layer. Several paths are currently explored to reduce significantly these contributions such as: the use of a laser emitting above 532 nm such as 575 nm (less energetic), the time-binning of the luminescence as the contribution from the silver ions would be faster than the NC photoluminescence, to the excitation of the NC via the waveguide (as opposed to from the top which is less efficient and thus requires more power) which would require less excitation power and thus less parasitic luminescence and finally the use of a pulsed excitation where again time-binning can be done and suppress the unwanted photoluminescence. Moreover, this work was using colloidal semiconductor quantum dots, but it paves the way towards more relevant emitters for quantum technologies such as colour centre in nanodiamonds where first results of positioning such nanoparticles using similar techniques as already been demonstrated[40].

Methods

Microphotoluminescence set-up

The microphotoluminescence (µ-PL) measurements were performed using a home-built setup based on an optical microscope in reflection mode. The samples were excited using a continuous-wave laser (picoquant LDH series) at a wavelength of 532 nm for the optical spectra. The same laser could be used in the pulsed mode for lifetime and $g^{(2)}(\tau)$ autocorrelation measurements. The excitation beam was focused onto the sample through a 100× objective with a numerical aperture of 0.95 (Olympus 100x Mplan Apo N), resulting in a spot size of around ~ 600 nm. The excitation power at the sample was kept below 100 µW to avoid local heating effects. The emitted photoluminescence was collected by the same objective in a backscattering configuration and directed to a spectrometer equipped with a 600 lines/mm grating (Princeton Instrument, model Isoplane 160 with proEM 1600 sensor). The signal was detected using a cooled CCD camera (Princeton Instrument, proEM 1600 sensor), providing a spectral resolution of approximately 0.9 meV at 600 nm. For lifetime and autocorrelation measurements, the emitted µ-PL was sent to a home-made HBT set-up with a 50/50 beamsplitter and two fibered APDs (EG&G/Excelitas, model AQRH-SPCM 14). The electronics and data analysis was done using a TCSPC electronics card (picoquant, mode picoharp series 300). All measurements were done at room temperature.

Nanocrystal synthesis

The synthesis of the nanocrystals was performed in two steps. First, the CdSe cores were obtained following the "Cao" method[41]. The estimation of the average core size and the concentration of the colloidal solution was obtained from the absorption spectrum of a diluted solution (10 µL in 3 mL of n-hexane), following[42,43], to find: R cores = 1,45 nm and C = 25,6 µM. From these data, shell growth was performed via the SILAR method and the resulting solution characterized in absorption and

photoluminescence[44,45]. The resulting NCs have oleic acid (OA) ligands, solubilized in n-hexane. Extinction coefficient from the core/shell structures at 350 nm was 1,72 × 10^6 $M^{-1}cm^{-1}$, estimated through the absorption spectrum under the assumption of conserved concentration between core & core/shell solutions.

One quarter of the NCs synthesis (2,5 mL) were introduced into a 250 mL tricol, with 10 g of trioctylphosphine oxide (TOPO) and 5 mL of tricoctylphosphine (TOP). The whole solution was heated under stirring until 70°C is reached, which melted the TOPO. The contents of the tricol were then degassed to evacuate the hexane and oxygen, before passing under argon atmosphere. The mixture was left under stirring for 1 h at 70°C. The resulting solution was then separated in 4 Falcon tubes of 50 mL and completed with ethanol. After centrifugation at 10 000 RCF for 5 min, the supernatant could be discarded and the precipitated NCs[TOP/TOPO] were resolubilised in toluene. The resolublisation in toluene was done with 2,5 mL to keep the concentration as unchanged as possible. Optical properties in solution were typically unchanged for this kind of ligand exchange.

Declaration statements:

(1) Data Availability: The datasets generated and/or analyzed during the current study are not publicly available as they are part of ongoing and future studies but are available from the corresponding author on reasonable request.

(2) Code Availability: not applicable

(3) Acknowledgements: The authors would like to thank the Graduate School (École Universitaire de Recherche) “NANO-PHOT”, contract ANR-18-EURE-0013, they acknowledge the use of the nano’mat platform from the CNRS Renatech network and funding from the FEDER, the Grand Est Region and the Aube Department. This work received support from French National Agency for Research-ANR of the OQuLuS project under the France 2030 initiative, contract ANR-23-PETQ-0013. The authors thank CNRS-Innovation and the SATT SAYENS for funding A. B. via the projects InteQ and InteQ2.

(4) Author Contributions: A. B. contributed to the fabrication and characterisation work and contributed significantly to the writing of the article, M. H. M. contributed to the characterisation and simulation work, N. R. contributed to the simulation work, A. H. contributed to the fabrication work, P. R. & C. V. contributed to the synthesis work, R. D. contributed to the data acquistion of the work, A. K. contributed to the discussions, S. B. contributed to the discussions, C. C. designed and supervised the work & contributed significantly to the writing of the article as well as the discussions. All authors reviewed the article.

(5) Competing Interests: The authors declare no competing interests.

References:

1. Couteau, C., Barz, S., Durt, T., Gerrits, T., Huwer, J., Prevedel, R., Rarity, J., Shields, A. & Weihs, G. Applications of Single Photons to Quantum Communication and Computing. *Nat. Rev. Phys.* 5, 326 (2023).

2. Couteau, C., Barz, S., Durt, T., Gerrits, T., Huwer, J., Prevedel, R., Rarity, J., Shields, A. & Weihs, G. Applications of Single Photons in Quantum Metrology, Biology and the Foundations of Quantum Physics. *Nat. Rev. Phys.* 5, 354 (2023).

3. Zhang, Y. et al. Experimental Single-Photon Quantum Key Distribution Surpassing the Fundamental Weak Coherent-State Rate Limit. *Phys. Rev. Lett.* 134, 210801 (2025).

4. Labonté, L. et al. Integrated Photonics for Quantum Communications and Metrology. PRX Quantum 5, 010101 (2024).

5. Pelucchi, E. et al. The Potential and Global Outlook of Integrated Photonics for Quantum Technologies. *Nat. Rev. Phys.* 4, 194 (2022).

6. Lounis, B. & Orrit, M. Single-Photon Sources. *Rep. Prog. Phys.* 68, 1129 (2005).

7. Beveratos, A., Kühn, S., Brouri, R., Gacoin, T., Poizat, J.-P., & Grangier, P. Room Temperature Stable Single-Photon Source. *Eur. Phys. J. D* 18, 191 (2002).

8. Morioka, N. et al. Spin-Controlled Generation of Indistinguishable and Distinguishable Photons from Silicon Vacancy Centres in Silicon Carbide. *Nat. Commun.* 11, 2516 (2020).

9. Chen, C. et al. Wavelength-tunable high-fidelity entangled photon sources enabled by dual Stark effects. *Nat. Commun.* 15, 5792 (2024).

10. Beltran Madrigal, J. et al. Hybrid Integrated Optical Waveguides in Glass for Enhanced Visible Photoluminescence of Nanoemitters. *Appl. Opt. 55*, 10263 (2016).

11. Lio, G. E. et al. Integration of Nanoemitters onto Photonic Structures by Guided Evanescent-Wave Nano-Photopolymerization. *J. Phys. Chem. C* 123, 14669 (2019).

12. Crespi, A. et al. Integrated Multimode Interferometers with Arbitrary Designs for Photonic Boson Sampling. *Nat. Photon.* 7, 545 (2013).

13. Yang, J. et al. Tunable quantum dots in monolithic Fabry-Perot microcavities for high-performance single-photon sources. *Light Sci. Appl.* 13, 33 (2024).

14. Redjem, W. et al. All-silicon quantum light source by embedding an atomic emissive center in a nanophotonic cavity. *Nat. Commun.* 14, 3321 (2023).

15. Liu, F. et al. High Purcell factor generation of indistinguishable on-chip single photons. *Nat. Nanotechnol.* 13, 835 (2018).

16. Riedrich-Möller, J., Arend, C., Pauly, C., Mücklich, F., Fischer, M., Gsell, S., Schreck, M. & Becher, C. Deterministic coupling of a single silicon-vacancy color center to a photonic crystal cavity in diamond. *Nano Lett.* 14, 5281 (2014).

17. Grandi, S. et al. Hybrid plasmonic waveguide coupling of photons from a single molecule. *APL Photonics* 4, 086101 (2019).

18. Senichev, A. et al. Silicon Nitride Waveguides with Intrinsic Single-Photon Emitters for Integrated Quantum Photonics. *ACS Photonics* 9, 3357 (2022).

19. Xie, W., Zhu, Y., Aubert, T., Hens, Z., Brainis, E., & Van Thourhout D. Fabrication and characterization of on-chip silicon nitride microdisk integrated with colloidal quantum dots. *Opt. Express* 24, A114 (2015).

20. Jeong, K.-Y., Lee, S. W., Choi, J.-H., So, J.-P. & Park, H.-G. Integration of Single-Photon

Emitters in 2D Materials with Plasmonic Waveguides at Room Temperature. *Nanomaterials* 10, 1663 (2020).
21. Alves, M. F. L. et al. Efficient guiding of quantum dot luminescence in CdS-doped phosphate glasses via femtosecond laser-written waveguides. Opt. & Laser Technol. 187, 112675 (2025).
22. Stas, P.-J. et al. Robust Multi-Qubit Quantum Network Node with Integrated Error Detection. *Science* 378, 557 (2022).
23. Aspuru-Guzik, A., & Walther, P. Photonic quantum simulators. *Nat. Phys.* 8, 285 (2012).
24. Wang, J., Sciarrino, F., Laing, A., & Thompson, M. G. Integrated Photonic Quantum Technologies. *Nat. Photon.* 14, 273 (2020).
25. Ramaswamy, R. V. & Srivastava, R. Ion-Exchanged Glass Waveguides: A Review. *J. Lightwave Technol.* 6, 984 (1988).
26. Tervonen, A., Honkanen, S. K. & West B. R. Ion-exchanged glass waveguide technology: a review. *Opt. Eng.* 50, 071107 (2011).
27. Nahra, M. et al. Single germanium vacancy centers in nanodiamonds with bulk-like spectral stability. *AVS Quantum Sci.* 3, 012001 (2021).
28. Khalid, A., Chung, K., Rajasekharan, R., Lau, D. W. M., Karle, T. J., Gibson, B. C. & Tomljenovic-Hanic, S. Lifetime Reduction and Enhanced Emission of Single Photon Color Centers in Nanodiamond via Surrounding Refractive Index Modification. *Sci. Rep.* 5, 11179 (2015).
29. Toninelli, C. et al. Single Organic Molecules for Photonic Quantum Technologies. *Nat. Mater.* 20, 1615 (2021).
30. Brokmann, X., Messin, G., Desbiolles, P., Giacobino, E., Dahan, M. & Hermier, J. P. Colloidal CdSe/ZnS Quantum Dots as Single-Photon Sources. *New J. Phys.* 6, 99 (2004).
31. Dabbousi, B. O. et al. (CdSe)ZnS Core–Shell Quantum Dots: Synthesis and Characterisation of a Size Series of Highly Luminescent Nanocrystallites. *J. Phys. Chem. B* 101, 9463 (1997).
32. Streltsov, A. M. & Borrelli, N. F. Study of Femtosecond-Laser-Written Waveguides in Glasses. *J. Opt. Soc. Am. B* 19, 2496 (2002).
33. Karasiński, P. & Rogoziński, R. Characterization and Sensor Properties of Sol–Gel SiO2:TiO2 Film/Ion-Exchange Glass Optical Waveguides. *Opt. Commun.* 281, 2472 (2008).
34. Xu, X. et al. Towards the Integration of Nanoemitters by Direct Laser Writing on Optical Glass Waveguides. *Photonics Res.* 8, 1541 (2020).
35. Wei, H., Pan, D., Zhang, S., Li, Z., Li, Q., Liu, N., Wang, W. & Xu, H. Plasmon Waveguiding in Nanowires. *Chem. Rev.* 118, 2882 (2018).
36. Weisser, M., Thoma, F., Menges, B., Langbein, U. & Mittler-Neher, S. Fluorescence in Ion Exchanged BK7 Glass Slab Waveguides and Its Use for Scattering Free Loss Measurements. *Opt. Commun.* 153, 27 (1998).
37. Hassanzadeh, A., Nitsche, M., Armstrong, S., Nabavi, N., Harrison, R., Dixon, S. J., Langbein, U. & Mittler, S. Optical Waveguides Formed by Silver Ion Exchange in Schott SG11 Glass for Waveguide Evanescent Field Fluorescence Microscopy: Evanescent Images of HEK293 Cells. *J. Biomed. Opt.* 15, 036018 (2010).
38. Galland, C., Ghosh, Y. Steinbrück, A., Sykora, M., Hollingsworth, J. A., Klimov V. I. & Htoon H. Two types of luminescence blinking revealed by spectroelectrochemistry of single quantum dots. *Nature* 479, 203 (2011).
39. Luo, Y. et al. On-Chip Hybrid Photonic–Plasmonic Light Concentrator for Nanofocusing in an Integrated Silicon Photonics Platform. *Nano Lett.* 15, 849 (2015).

40. Issa, A. et al. One Strategy for Nanoparticle Assembly onto 1D, 2D, and 3D Polymer Micro and Nanostructures. *ACS Appl. Mater. Interfaces* 13, 41846 (2021).
41. Yang, Y. A., Wu, H., Williams, K. R., & Cao, Y. C. Synthesis of CdSe and CdTe Nanocrystals without Precursor Injection. *Angew. Chem.* 44, 6712 (2005).
42. Leatherdale, C. A., Woo, W. K., Mikulec, F. V., & Bawendi, M. G. On the Absorption Cross Section of CdSe Nanocrystal Quantum Dots. *J. Phys. Chem. B* 106, 7619 (2002).
43. Yu, W. W., Qu, L., Guo, W., & Peng, X. Experimental Determination of the Extinction Coefficient of CdTe, CdSe, and CdS Nanocrystals. *Chem. Mater.* 15, 2854 (2003).
44. Li, J. J., Wang, Y. A., Guo, W., Keay, J. C., Mishima, T. D., Johnson, M. B., & Peng, X. Large-Scale Synthesis of Nearly Monodisperse CdSe/CdS Core/Shell Nanocrystals Using Air-Stable Reagents via Successive Ion Layer Adsorption and Reaction. *J. Am. Chem. Soc.* 125, 12567 (2003).
45. Xie, R., Kolb, U., Li, J., Basché, T., & Mews, A. Synthesis and Characterization of Highly Luminescent CdSe−Core CdS/Zn0.5Cd0.5S/ZnS Multishell Nanocrystals *J. Am. Chem. Soc.* 127, 7480 (205).

Fig. 1 | Schematic of the integrated single photon source. Schematic of the integrated single photon source based on an ion-exchange waveguide (IEW) which allows to propagate and guide the photons emitted from a single nanocrystal (NC) thanks to the coupling with a secondary waveguide made of titanium dioxide-TiO_2.

Fig. 2 | Nanocrystals optical properties. a normalised absorption and photoluminescence of cores/shells NCs. **b** Second order correlation function $g^{(2)}(\tau)$ for a single core/shell NC with a pulsed excitation laser at 532 nm (gray area: background light emission).

Fig. 3 | Fabrication of the TiO_2 waveguides. TiO_2 fabrication process on our photonics platform, followed by the functionalization of NCs on TiO_2 strip waveguides (not to scale).

Fig. 4 | **Microphotoluminescence set-up.** Microphotoluminescence set-up used for optical characterisation, with a CW or pulsed 532 nm laser as a source of excitation.

Fig. 5 | Microphotoluminescence scan image. 10 µm by 40 µm photoluminescence scan image of a TiO_2 structure on an ion-exchange waveguide with a single NC emitting. Excitation is done at 532 nm with a bandpass filter 650 $\pm$ 75 nm.

Fig. 6 | Optical properties of the integrated single photon source. a Photoluminescence from the NC from identified in Fig. 5: in black the spectrum is measured on top of the IEW-TiO_2, structure, in blue is the residual fluorescence coming from the IEW-TiO_2 structure and in red is the fluorescence at the fibre end with an excitation laser at 532 nm (orange area represents the bandwidth of the filter used for HBT), **b** second order correlation function for the single NC on top of the IEW-TiO_2 structure excited from the top with a pulsed excitation and collected from the fibre connected to the waveguide (in gray: background level due to broad filtering).

Fig. 7| Nanocrystal lifetime measurements. In black is the average lifetime measurement of 10 single NCs on a glass substrate alone and in red is the average lifetime measurement of 3 single NCs on the IEW/TiO_2 photonic structure.

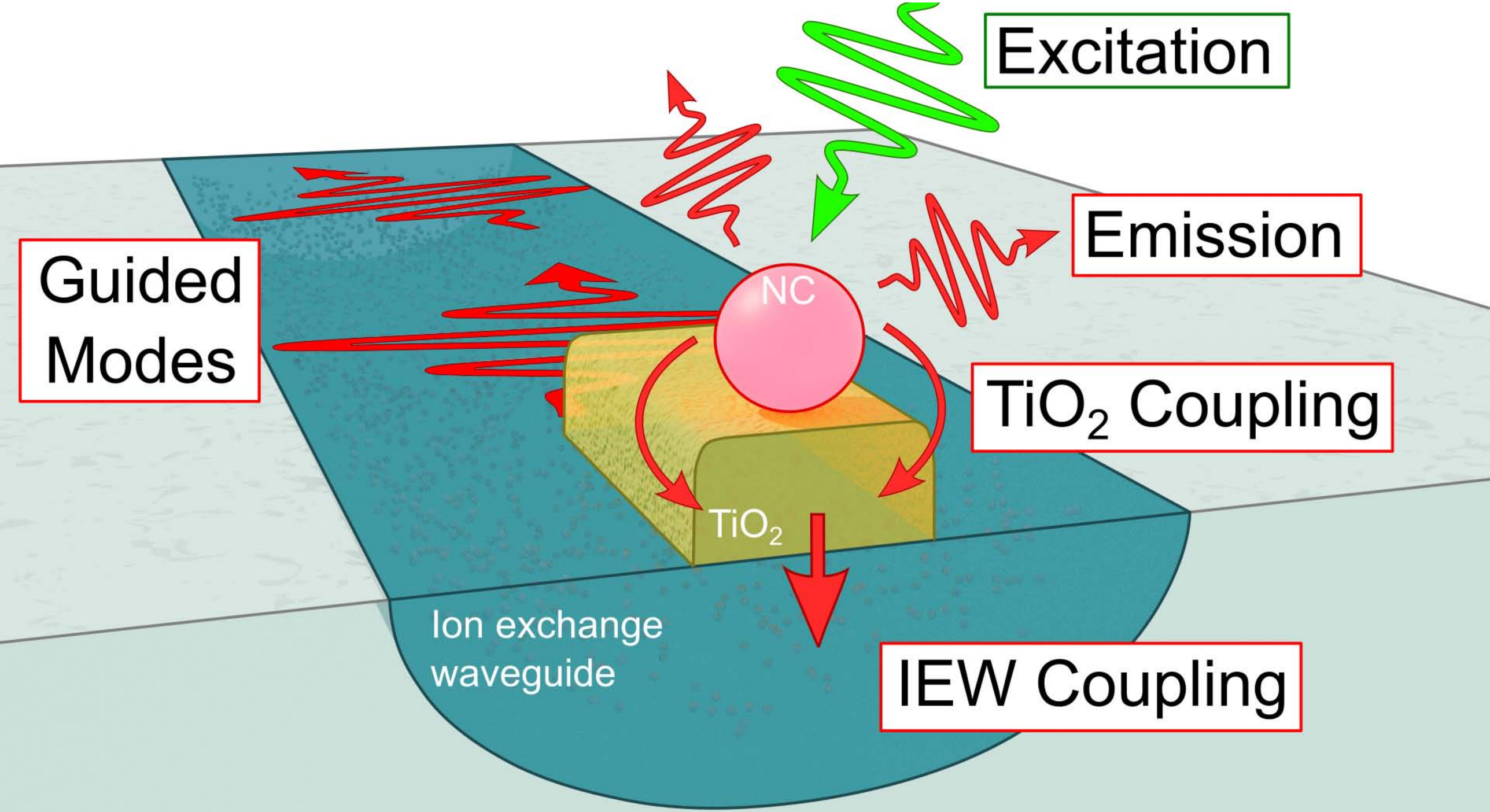
Excitation
Emission
Guided Modes
NC
TiO2 Coupling
TiO2
Ion exchange waveguide
IEW Coupling

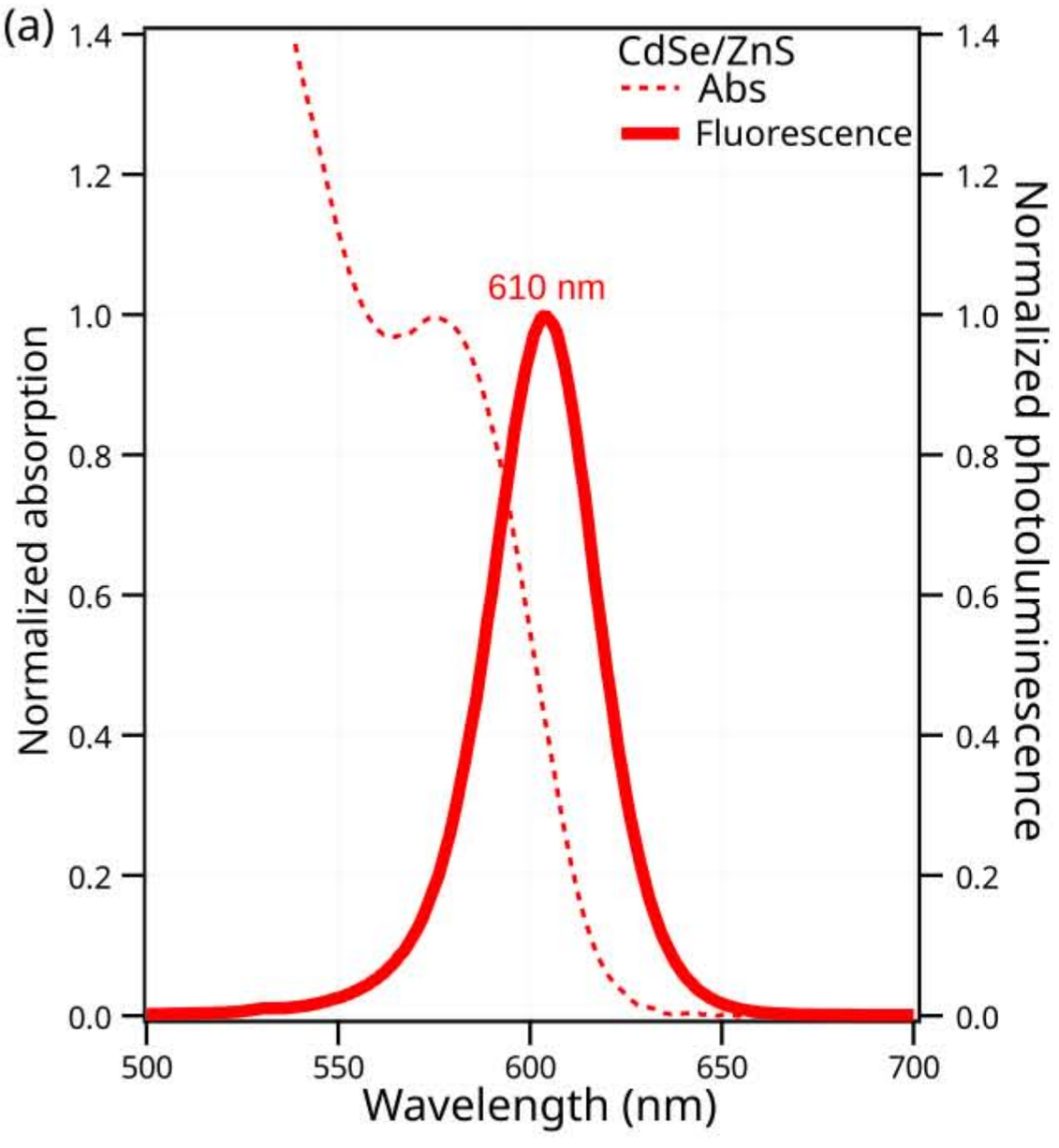
(a)
CdSe/ZnS
Abs
Fluorescence
610 nm
Normalized absorption
Normalized photoluminescence
Wavelength (nm)
0.0
0.2
0.4
0.6
0.8
1.0
1.2
1.4
500
550
600
650
700

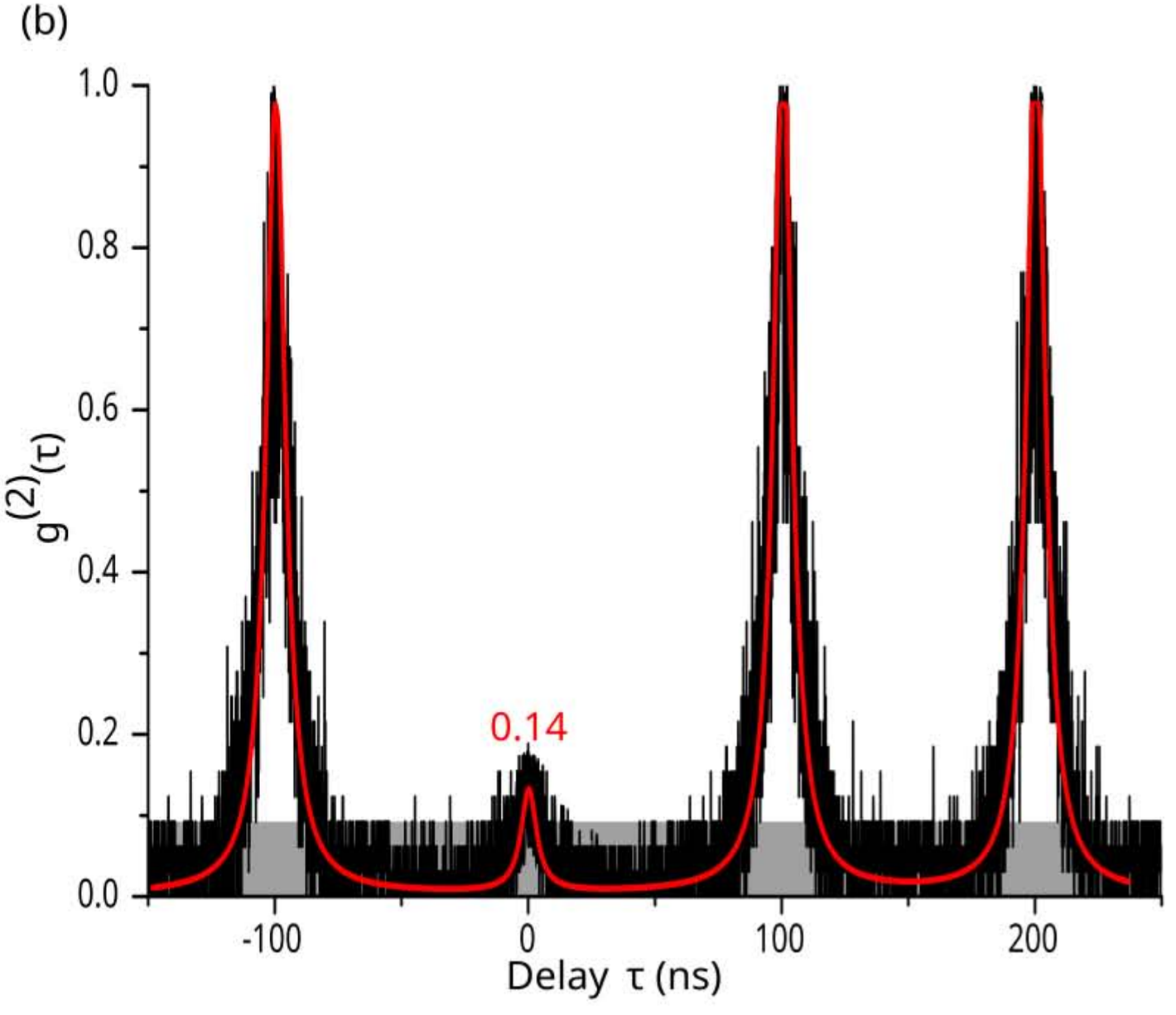
(b)
$g^{(2)}(\tau)$
0.14
Delay τ (ns)
0.0
0.2
0.4
0.6
0.8
1.0
-100
0
100
200

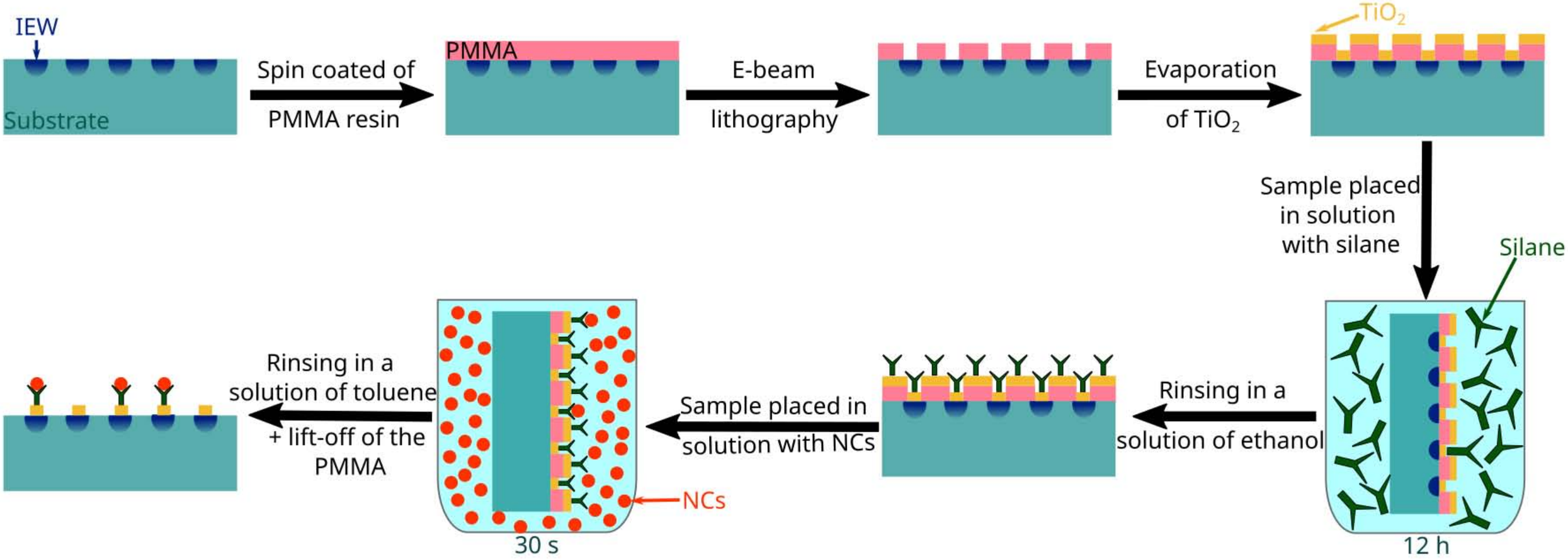
IEW
Substrate
Spin coated of
PMMA resin
PMMA
E-beam
lithography
Evaporation
of TiO2
TiO2
Sample placed
in solution
with silane
Silane
12 h
Rinsing in a
solution of ethanol
Sample placed in
solution with NCs
NCs
30 s
Rinsing in a
solution of toluene
+ lift-off of the
PMMA

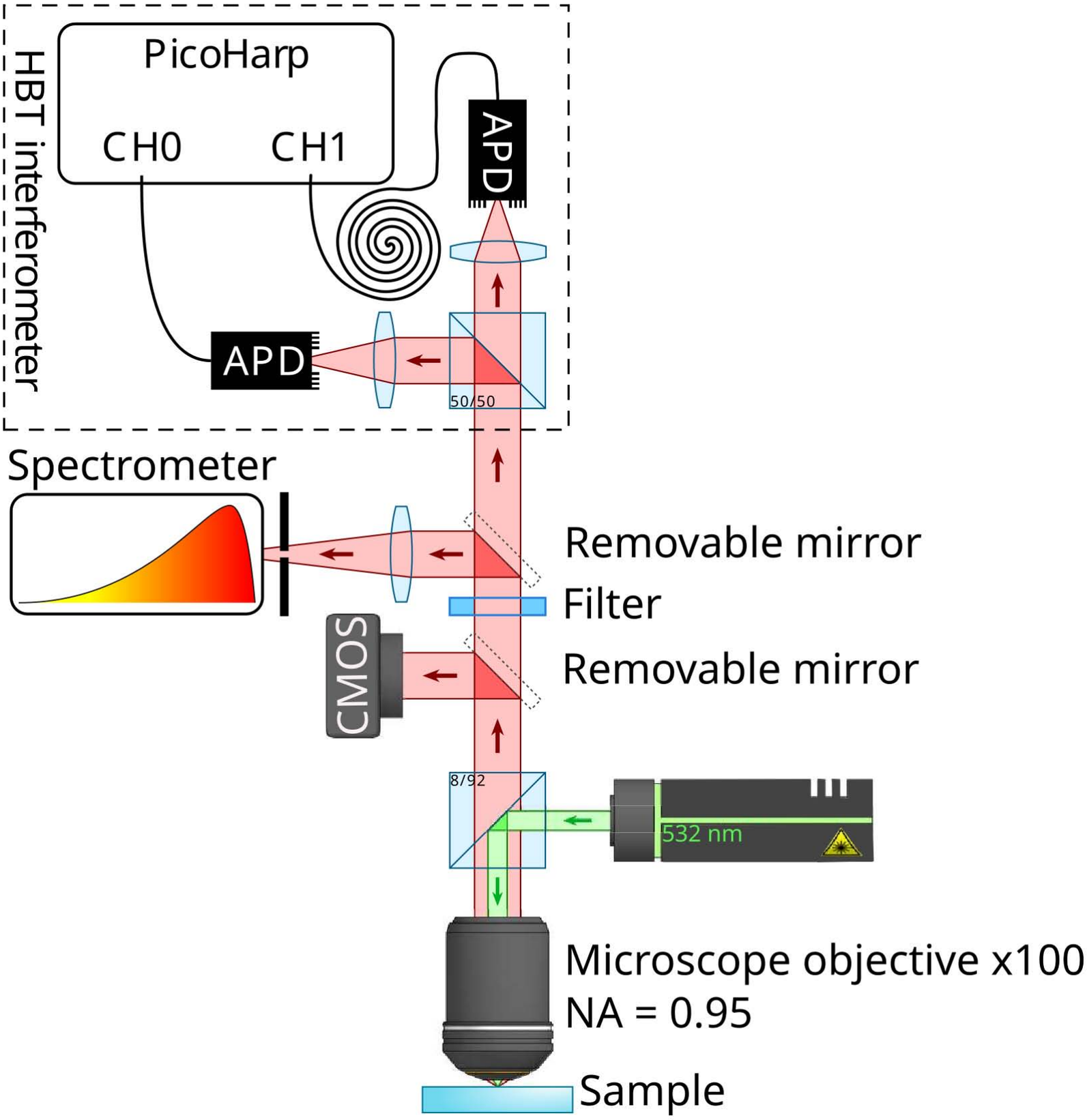
HBT interferometer
PicoHarp
CH0
CH1
APD
APD
50/50
Spectrometer
Removable mirror
Filter
CMOS
Removable mirror
8/92
532 nm
Microscope objective x100
NA = 0.95
Sample

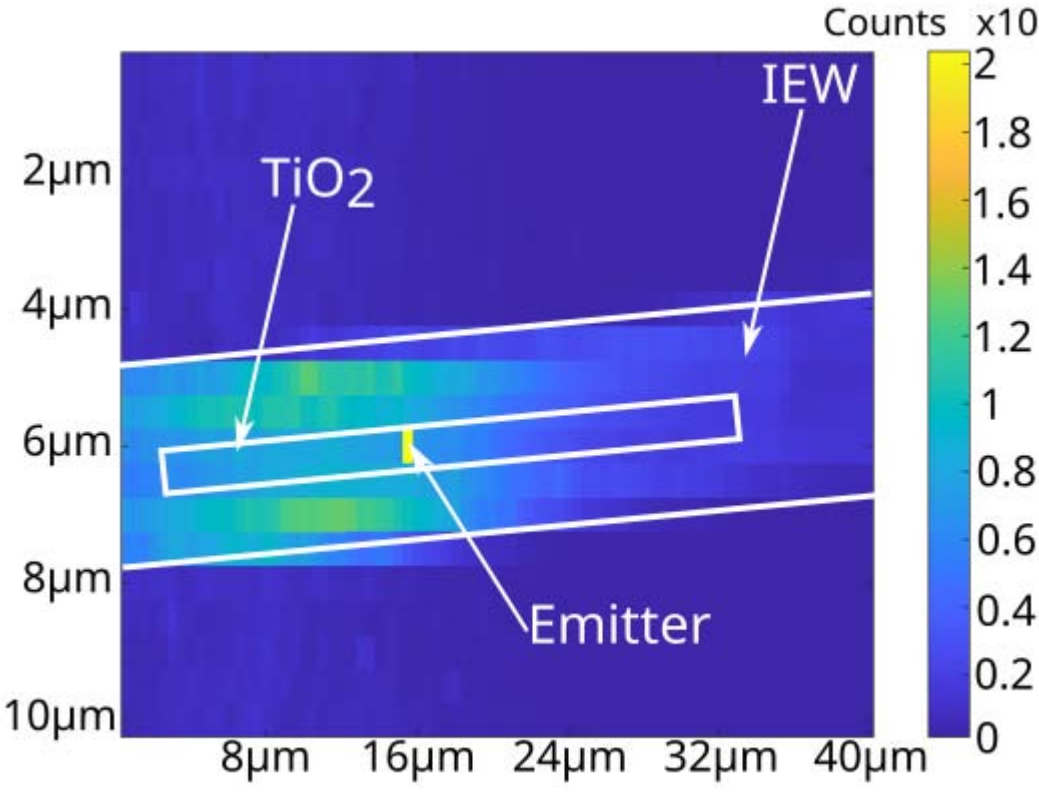
Counts
x10
2
1.8
1.6
1.4
1.2
1
0.8
0.6
0.4
0.2
0
IEW
TiO2
Emitter
2µm
4µm
6µm
8µm
10µm
8µm
16µm
24µm
32µm
40µm

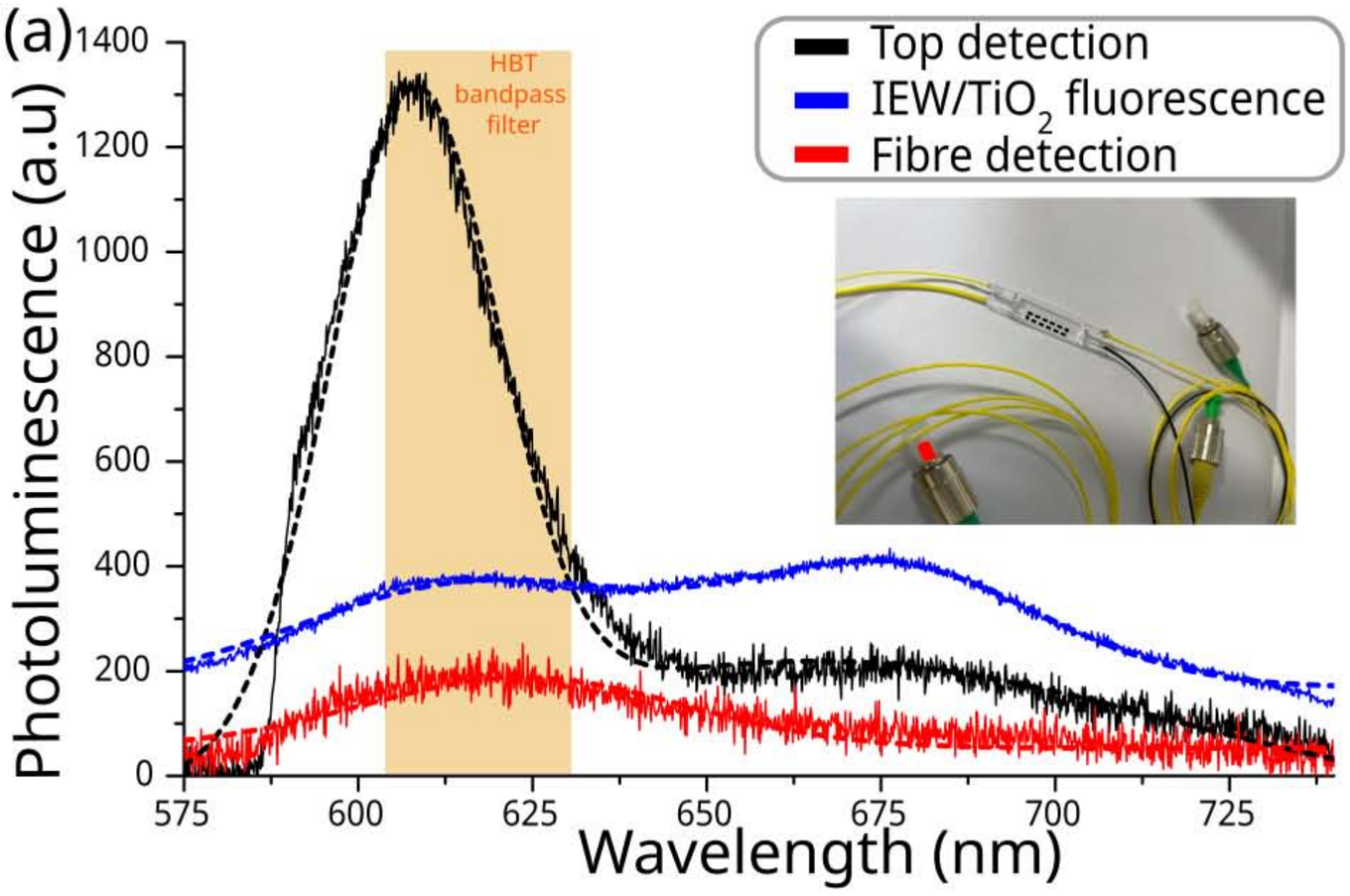
(a)
Photoluminescence (a.u)
Wavelength (nm)
HBT bandpass filter
Top detection
IEW/TiO2 fluorescence
Fibre detection
0
200
400
600
800
1000
1200
1400
575
600
625
650
675
700
725

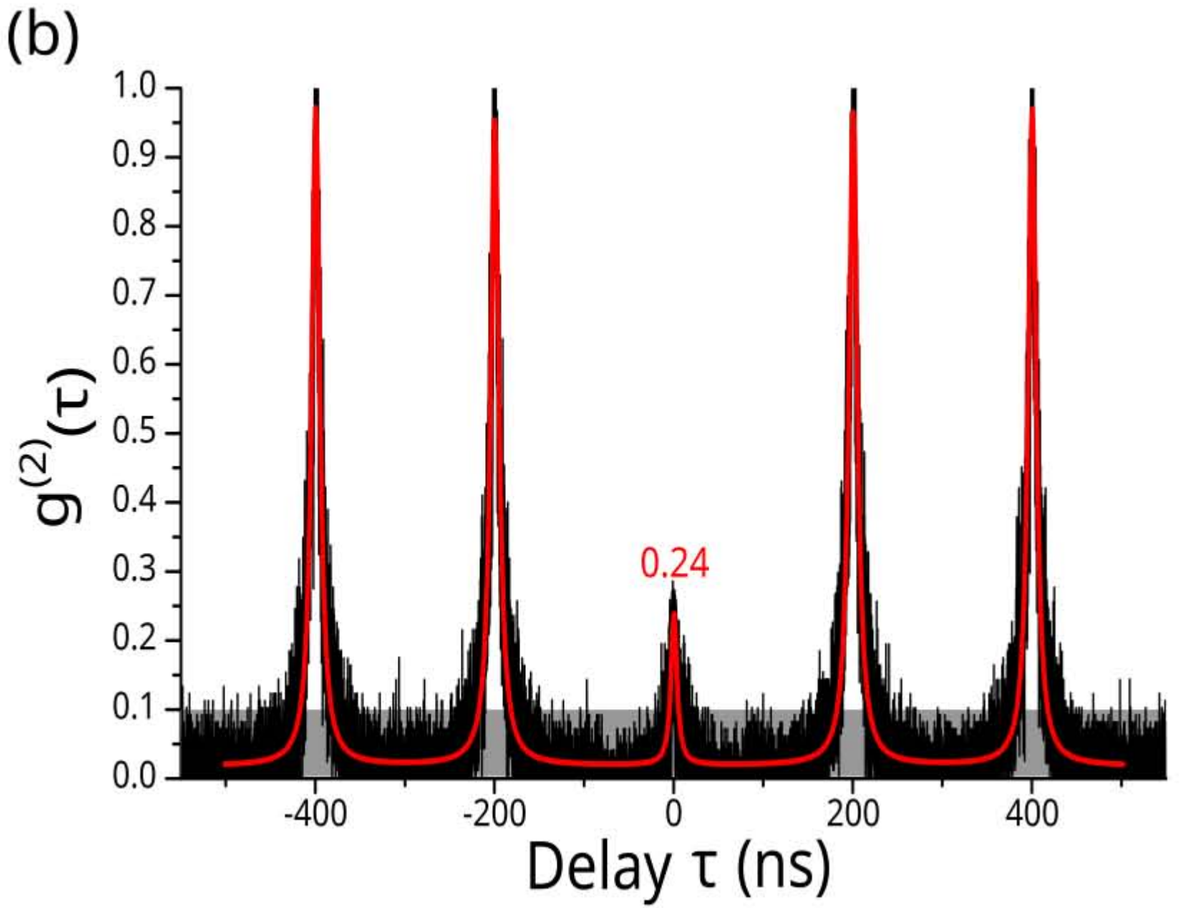
(b)
g(2)(τ)
Delay τ (ns)
0.24
0.0
0.1
0.2
0.3
0.4
0.5
0.6
0.7
0.8
0.9
1.0
-400
-200
0
200
400

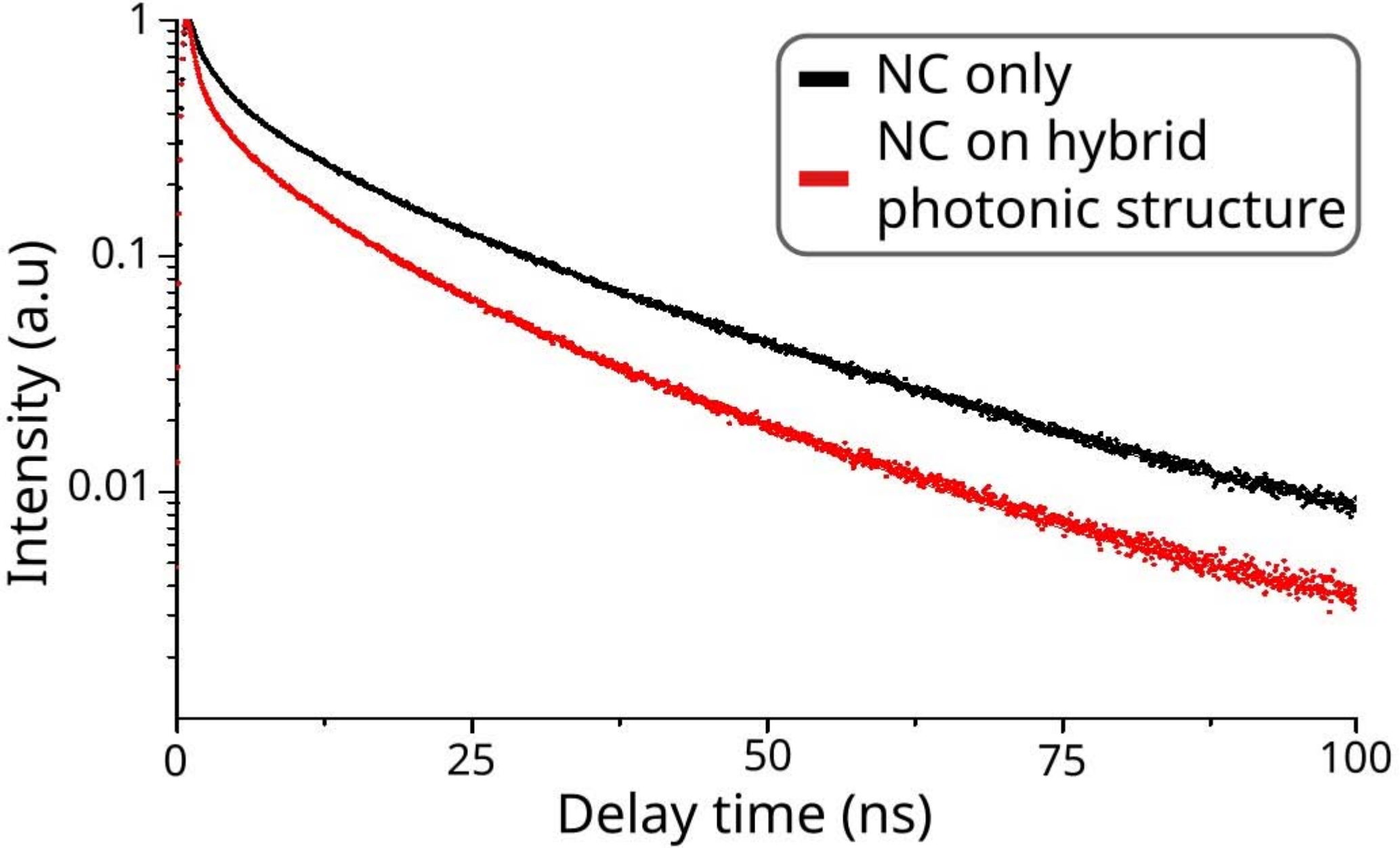
NC only
NC on hybrid photonic structure
Intensity (a.u)
1
0.1
0.01
0
25
50
75
100
Delay time (ns)